NASA TECHNICAL TRANSLATION NASA TT F-15,931

CONTRUCTION AND CALIBRATION OF A NEUTRON SPECTROMETER IN THE ENERGY RANGE OF 10-50 MeV

I. Böhm, J. Böhm and G. Wibberenz

Translation of "Aufbau und Eichung eines Neutronenspektrometers im Energiebereich von 10 MeV bis 50 MeV", Atomkernenergie (ATKE), Vol. 21, No. 1, 1973, pp. 48-54.

(NASA-TT-F-15931) CONSTRUCTION AND CALIBRATION OF A NEUTRON SPECTROMETER IN THE ENERGY RANGE OF 10-50 MeV (Scientific Translation Service) 26 p HC $4.50 CSCL 14B G3/14

N74-33947

Unclas 49303

NATIONAL AERONAUTICS AND SPACE ADMINISTRATION
WASHINGTON, D. C. 20546 SEPTEMBER 1974

STANDARD TITLE PAGE

1. Report No. NASA TT F-15,931	2. Government Accession No.	3. Recipient's Catalog No.
4. Title and Subtitle: Construction and calibration of a neutron spectrometer in the energy range of 10-50 MeV		5. Report Date: September, 1974 6. Performing Organization Code
7. Author(s): I. Böhm, J. Böhm and G. Wibberenz		8. Performing Organization Report No. 10. Work Unit No.
9. Performing Organization Name and Address: SCITRAN, Box 5456, Santa Barbara, CA 93108		11. Contract or Grant No. NASw-2483 13. Type of Report and Period Covered: Translation
12. Sponsoring Agency Name and Address: National Aeronautics and Space Administration, Washington, D.C. 20546		14. Sponsoring Agency Code

15. Supplementary Notes

Translation of "Aufbau und Eichung eines Neutronenspektrometers im Energiebereich von 10 MeV bis 50 MeV", Atomkernenergie (ATKE), Vol. 21, No. 1, 1973, pp. 48-54.

16. Abstract

The construction and calibration of a neutron spectrometer for measuring solar neutrons is described. A simple circuit is given for electronic separation of gamma rays and neutrons. Inelastic interactions of neutrons with energy of 18 MeV and more with carbon atoms can no longer be neglected in the scintillator NE 213 used here for neutron detection.

17. Key Words (Selected by Author(s))	18. Distribution Statement: Unclassified - Unlimited		
19. Security Classif. (of this report): Unclassified	20. Security Classif. (of this page): Unclassified	21. No. of Pages: 26	22. Price

CONSTRUCTION AND CALIBRATION OF A NEUTRON SPECTROMETER IN THE ENERGY RANGE OF 10-50 MeV

I. Böhm, J. Böhm and G. Wibberenz

1. Introduction

/ 48 *

The neutron spectrometer described in this work was planned in order to demonstrate solar neutrons at the top of the atmosphere. Such neutrons were first predicted by Biermann, Haxel and Schlüter (1951). There are various reasons for a particular interest in the measurement of solar neutrons. For one, it is hoped that conclusions can be drawn on the mechanisms of acceleration near the Sun in flares from the measured neutrons. As neutrons are also not deflected by the interplanetary magnetic field, one can, by simultaneous measurement of neutrons and protons from a flare near the Earth, draw conclusions about the properties of interplanetary space (see Roelof, 1966). Another interesting aspect is the question of the extent to which the protons of the radiation belt are generated by decay of neutrons. Neutrons from the Sun (Claflin and White, 1970) and the albedo neutrons generated in the atmosphere of the Earth (Farley, Tomassian and Walt, 1970) could play a part in this. Chupp (1971) presents a recent review article on solar neutrons. The search for solar neutrons has been unsuccessful up to the present, however. It has been possible only to state upper limits for the fluxes of solar neutrons. The measurements are so difficult because the neutron flux to be demonstrated is small and the response of the instruments is only of the order of a few percent or lower (see, for instance, Göllnitz et al., 1969).

---

* Numbers in the margin indicate pagination in the original foreign text.

One measuring principle used in many cases is the demonstration of neutrons through nuclear reactions in scintillators, which consist predominantly of hydrogen and carbon. In the present case, the liquid scintillator NE 213 was used in a vessel of 10 x 10 x 10 cm^3. At high energies, not only the reactions with hydrogen but also those with carbon play a part in demonstration of the neutrons. That means that in calculating the response capability of the apparatus, one must, aside from the recoil protons arising in the H reactions, also pay quite special attention to the secondary particles from the C reactions. Only a few statements appear in the literature on the energy dependence of the effective cross section for inelastic scattering of neutrons at carbon and on the secondary products which appear there (Bowen, Cox et al., 1962; Hunt, Baker et al., 1970; Edelstein, Russ et al., 1972).

One method which is generally common and which is also used here is to eliminate charged particles by means of an anticoincidence scintillator surrounding the demonstration scintillator. In this method, however, gamma quanta which penetrate the anticoincidence scintillator can simulate neutrons in the demonstration scintillator.

In the present work, two subjects are treated particularly intensively. For one thing, we describe an electronic pulse shape discrimination method which we ourselves developed for the apparatus. It makes it possible to separate neutrons from gamma quanta (compare also the methods developed by Kinbara and Kumahara, 1969, and by Onge and Lockwood, 1969). Also, we specially consider the role of carbon in neutron demonstration, the problem which was mentioned above. Through analysis of the pulse height spectra generated in the apparatus from calibration neutron spectra, one arrives at important conclusions on the importance of carbon in calculating the detection probability.

This article is the continuation of studies on separation of neutrons and gamma quanta in the energy range from 1 to 10 MeV by means of electronic pulse shape discrimination methods (Busse, 1967).

2. Construction of the Apparatus

Figure 1 gives a schematic section through the spectrometer. The units for electronic pulse processing are not shown. The central part of the counter is the vessel containing the liquid scintillator, NE 213, which is used to discriminate between weakly and strongly ionizing particles. The 14-dynode multiplier, 56 AVP views the liquid from the only side not covered with a reflecting paint. Both the 56 AVP and the NE 213 vessel are enclosed in a light-tight aluminum cylinder and are pushed into a Ne 102a plastic scintillator which is 2 cm thick on all sides. / 49

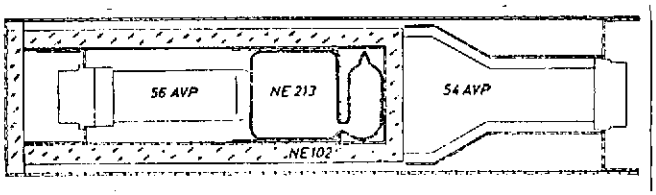

Figure 1. Cross-section of the neutron spectrometer. The arrangement of the detection scintillator, NE 213, the anticoincidence scintillator, NE 102, and the two multipliers, 56 AVP and 54 AVP, can be seen.

This cylinder of NE 102a, which is observed by a Type 54 AVP multiplier with an 11 cm cathode, serves to identify all the charged particles, which are excluded from recording through anticoincidence. The outer scintillator, with its multiplier, is also enclosed in a light-tight aluminum tube. Figure 2 shows

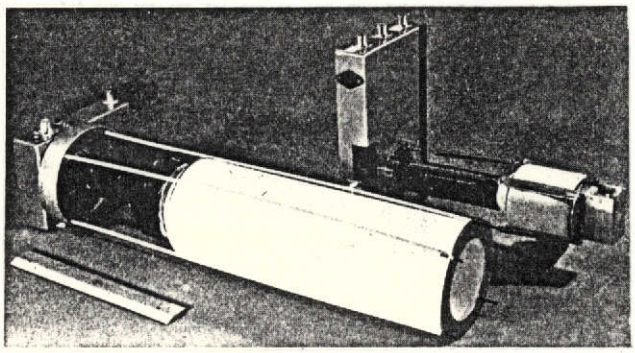

Figure 2. The neutron spectrometer with the NE 213 detection scintillator removed.

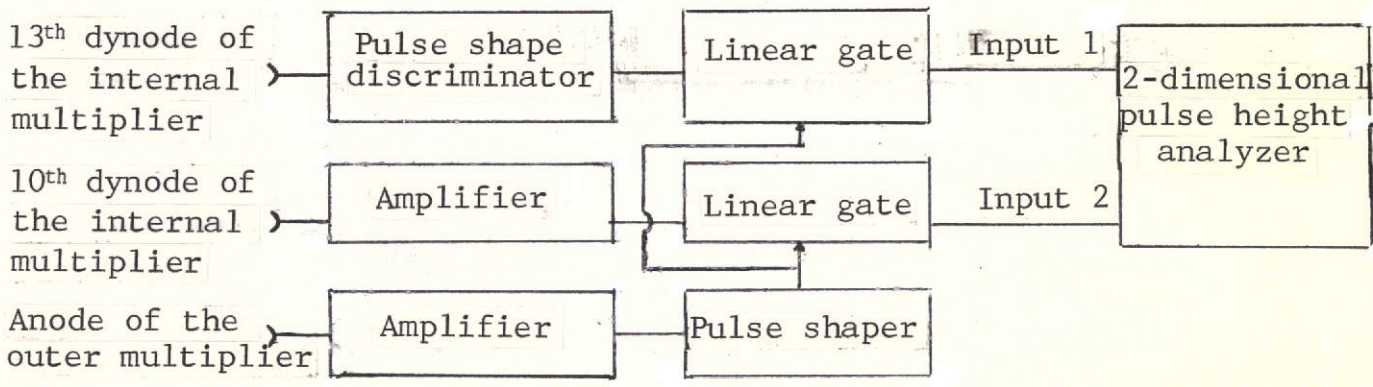

Figure 3. Block diagram of the neutron spectrometer.

the two scintillators, which can be slid together, with their multipliers without light shielding. The NE 213 vessel has a length and a diameter of 10 cm each. The Ne 102 a can is 44 cm long, has a clear diameter of 11 cm, and, with a wall thickness of 2 cm, has an outside diameter of 15 cm.

Figure 3 shows the block diagram for the experiment. A 56 AVP photomultiplier is used to detect the light flashes in the inner scintillator. The pulses for pulse shape discrimination are taken from its 13th dynode. Pulses from

neutrons have lower negative undershoots and larger positive amplitudes than pulses from gamma quanta with the same light yield. The pulses from the tenth dynode are proportional to the energies of the incident particles and are amplified linearly. The anode pulses are taken from the 54 AVP multiplier, which observes the outer scintillator, and highly amplified. These pulses trigger a pulse shaper having a response threshold only a little above the noise of the 54 AVP. The output pulses from the pulse shaper close two linear gates for 10 μs, so that no pulse shape discriminator and energy pulses can get through the gates during this period. This anticoincidence circuit eliminates charged particles incident on the apparatus from outside. All pulses which get through the gates are recorded in a 2-dimensional pulse height analyzer, with the undershoots of the pulse discriminator pulses cut off. This gives a 2-dimensional spectrum in which the neutrons and gamma quanta are separated in different "branches".

3. Calibration of the Apparatus with Two Known Neutron Spectra

3.1 Generation of the Neutron Spectra

Schweimer (1966) measured the neutron emission of thick targets in the forward direction using a time of flight method. In order to ensure obtaining the same spectra for calibration of the neutron spectrometer, we used the same generation mechanism for the neutrons as in the measurements by Schweimer (Figure 4).

In the sector-focusing cyclotron at Karlsruhe, 46.35 MeV deutrons were generated and used to irradiate various thick targets. A thin aluminum foil was held in front of the water-cooled clamping target head to check on the beam current integral. The neutron spectrum resulting from irradiation of the thick

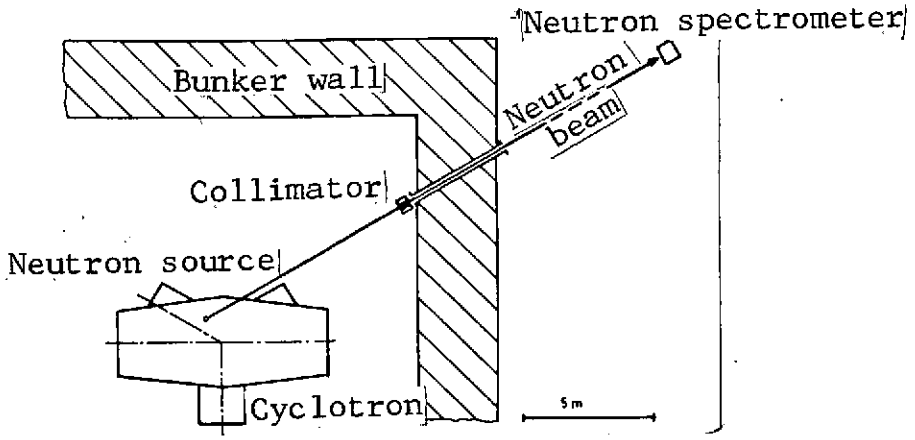

Figure 4. Path of the neutron beam at the cyclotron in Karlsruhe.

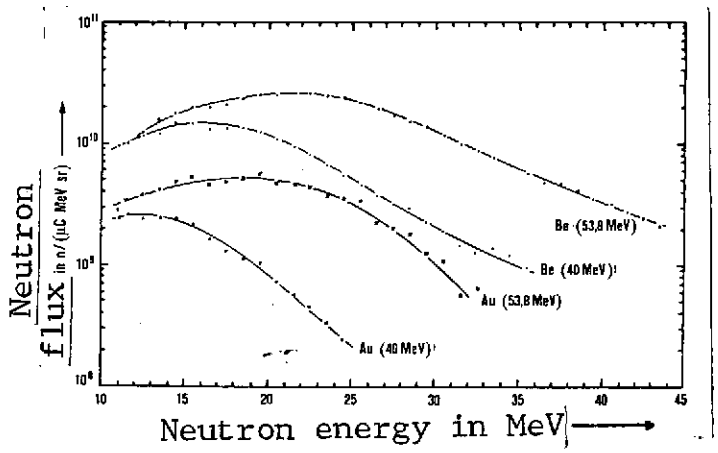

Figure 5. The neutron spectra used for calibration of the neutron spectrometer (after Schweimer, 1966). These spectra were produced by irradiation of thick Au or Be targets with deuterons of 40 and 53.8 MeV.

target was collimated through an iron cube with a 25 cm edge length, with an aperture of 26 x 40 mm^2 cross section, striking the apparatus at a distance of 57 m from the neutron source. By bombarding Be and Au targets with energies of 40 and 53.8 MeV, respectively, one obtains the spectra of Figure 5, according to Schweimer.

3.2 Measuring Arrangement During Calibration

Differing from Figure 1, the shielding scintillator, NE 102, was left out in the calibration measurements and only the inner scintillator, NE 213, was exposed to the neutron flow. This did not falsify the measurement in this case, because the neutron flux was considerably greater than the background of charged particles from the environment. Furthermore, the proportion of charged secondary particles which arise in a neutron collision and leave the scintillator is, at $E_n = 40\,\text{MeV} \gtrsim 10\%$ and, for instance, at $E_n = 20\,\text{MeV} \gtrsim 2\%$, so that this effect can be neglected, because the calibrating neutron spectra extend to some 40 MeV and rise steeply at lower energies. / 50

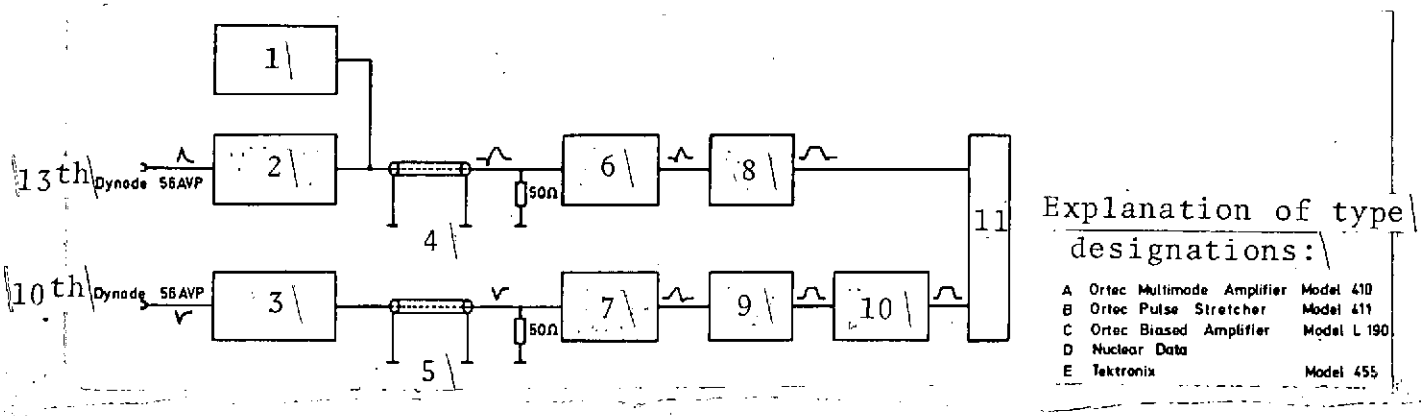

Figure 6. Block diagram of the measuring arrangement at the cyclotron.

1 - Type E oscillograph
2 - Pulse shape discriminator according to Figure 7
3 - Impedance converter
4 - 100 m coaxial cable
5 - 100 m coaxial cable
6 - Type A linear amplifier
7 - Type A linear amplifier
8 - Type B stretcher
9 - Type B stretcher
10 - Type C linear amplifier
11 - Type D 2-dimensional pulse height analyzer

Figure 6 contains the block diagram for the measuring arrangement at the cyclotron. After the pulses from the 13-th dynode of the 56 AVP are processed in the pulse shape discriminator, they arrive at the 50 ohm coaxial cable, some 100 m long, which connects the measuring room with the cyclotron. There the discriminator pulses are linearly amplified and then

brought to a peak length of 1 μs with a stretcher. In this stretching the negative undershoots are cut off. The pulses stretched in this manner arrive at an analog-digital converter of the 2-dimensional multichannel analyzer. The energy pulses from the tenth dynode of the 56 AVP are obtained with an emitter follower of low source impedance and are also conducted to the measuring room over a 50 ohm coaxial cable some 100 m long. There they are linearly amplified, integrated with a time constant of 0.5 μs, and then stretched to 1 μs peak length. They are amplified again and then analyzed in the second analog-digital converter of the multichannel analyzer. The 2-dimensional spectrum can be seen directly on a viewing screen of the multichannel analyzer.

3.3 Separation Between Gamma Quanta and Neutrons

The separation had been done previously up to neutron energies of 8 MeV (see Busse, 1967); but above this energy threshold the circuits reported there failed. But, as the principle of pulse shape discrimination must apply also at high energies, the circuit of Figure 7 was developed. In this circuit, the pulses derived from the original pulses at the 13th dynode could be converted into both integrated and differentiated forms. The two could be summed, with weighting, after stretching and inversion of the differentiated pulse. The extent of integration and differentiation and the weighting of the summation could each be controlled by a special potentiometer, INT, DIF and ADD. These potentiometers (Amphenol Micropot Type 2901) are adjustable metal film resistances, so that in the present circuit, pulse rise times $\gtrsim$ 20 ns could still be transmitted satisfactorily. The printed circuit for the discriminator, the plan for which is shown in Figure 8, was made in a circle so that it could fit into the anticoincidence scintillator.

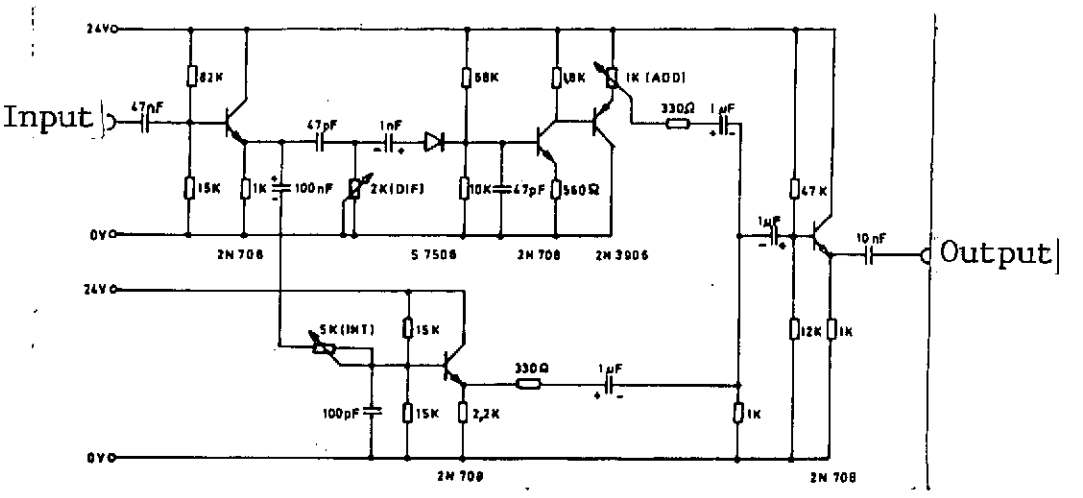

Figure 7. Circuit diagram of the pulse shape discriminator.

Figure 8. Plan of the printed circuit for the pulse shape discriminator of Figure 7.

For adjustment of the separation of gamma quanta and neutrons, a thick Cu target was irradiated with 46.35 MeV deuterons and the 2-dimensional spectrum was observed on the multichannel analyzer. In this case, copper is particularly suitable as the target because relatively many gamma quanta are produced along with the neutrons, so that one can observe the quality of the separation after irradiation of the apparatus for only some 5 minutes. The positions of the INT, DIF and ADD potentiometers were varied until distinct separation was obtained above 20 MeV. The Tektronix Type 455 oscilloscope (150 MHz bandwidth) gave valuable help in these adjustments, because the output of the pulse shape discriminator could be monitored directly with it. The quality of the separation depends heavily on V_{up}, the ratio of the undershoot to the pulse amplitude, and also on the duration, D, of the undershoot. Good separation was obtained with an adjustment with the following values for muons:

$V_{up} = 1.0$ D = 30 ns

3.4 Measurement of the Calibration Neutron Spectra

/ 51

After it has been ascertained that a distinct separation was obtained above 20 MeV, one Be and one Au target were irradiated with deuterons. The deuteron current integral was determined from an 100 μ aluminum foil clamped in front of the target head. The current integral was determined by determining the amount of ^{22}Na or ^{24}Na produced in the irradiation. The effective cross sections $\sigma_{^{22}Na}$ and $\sigma_{^{24}Na}$ for production of ^{22}Na and ^{24}Na are known. This yields the total number of incident deuterons. The following table shows a summary of the measurements:

Table:

	Be-irradiation	Al-irradiation
Irradiation time, minutes	13	27
Deuteron beam current, nA	15	24
$\sigma_{^{22}Na}$ in mb	44	44
$\sigma_{^{24}Na}$ in mb	27.1	27.1
Number of deuterons, based on the ^{22}Na measurement = D_1	$2.4 \cdot 10^{13}$	$10.9 \cdot 10^{13}$
Number of deuterons, based on the ^{24}Na measurement = D_2	$4.66 \cdot 10^{13}$	$21 \cdot 10^{13}$

The value of $\sigma_{^{22}Na}$ for E_d = 46.3 MeV was derived from the known value for E_d = 53.8 MeV [$\sigma_{^{22}Na}$ (53.8 MeV) = 32 mb], assuming that the energy curve of $\sigma_{^{22}Na}$ is equal to the well known curve for $\sigma_{^{24}Na}$. Thus, the deuteron number from the ^{24}Na measurement is more accurate. The differential pulse height spectrum, dh/dk for the energy pulses, was measured in 64 channels of k, and is shown in Figure 9 for Be and Au. The pulse heights are a measure for the energy given off in the scintillator by the protons and other secondary particles generated by the neutrons. There is, however, no linear relation between the proton energy and the light yield of the scintillator, such as has been measured for gamma quanta, for instance. For gamma energies $E_\gamma > 3$ MeV, referred to the same light yield, the following relation to the proton energy, E_p, was used:

$$E_\gamma = 0.6\ E_p - 1.28 \quad (E_p, E_\gamma \text{ in MeV})$$

Thus, a gamma quantum of 4.7 MeV generates a light flash which is just as bright as that from a proton of 10 MeV. By

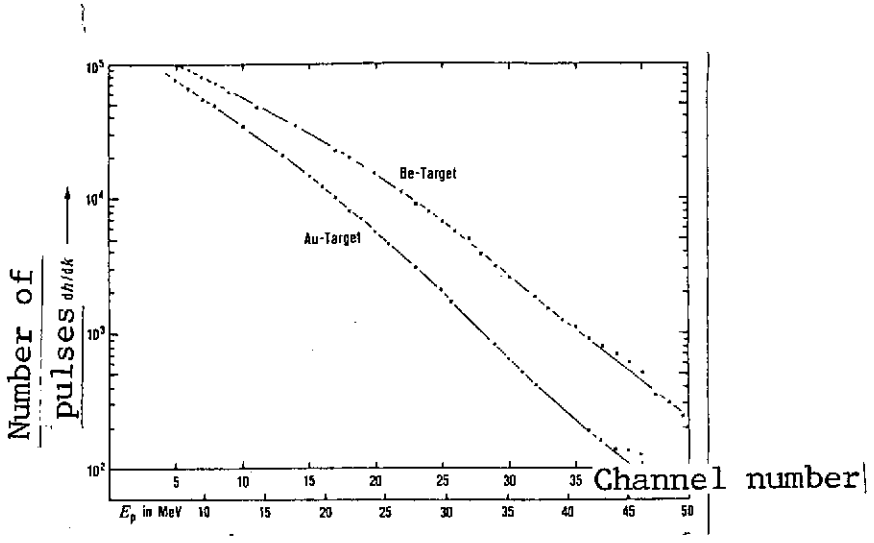

Figure 9. Measured differential pulse height distribution, dh/dk, of the energy pulses of the neutron spectrometer during the irradiation of the apparatus with two neutron spectra. The neutron spectra were produced by irradiation of Au and Be targets with 46.3 MeV deuterons.

means of this relation, we could undertake the energy calibration of the dh/dk spectrum of Figure 9.

Qualitatively, one notes a weaker drop-off of the energy pulse spectrum toward higher energies for Be than for Au. This is also to be expected according to the neutron spectra of Figure 5, because these spectra have the same tendency above 15 MeV.

4. Theoretical Calculation of the Secondary Spectrum Produced by a Known Neutron Spectrum

As neutrons have no electrical charge, their electromagnetic interaction with matter is extremely weak. The most important reactions of the neutrons are nuclear collisions of elastic and inelastic types. Hydrogen-containing material

is particularly well suited for determination of neutron energies because the nuclear collisions with protons can be observed relatively well, as they are expressed primarily in a change in the direction of the original neutron flight path and in a corresponding energy loss.

But the scintillator contains a non-negligible proportion of C atoms along with the H atoms. The neutrons enter into inelastic, as well as elastic, interactions with them. Among others, the following reactions come into consideration for inelastic collisions of neutrons with carbon:

$$\left.\begin{array}{l} C^{12}(n,\alpha)Be^{9} \\ C^{12}(n,n')C^{12*}(3\alpha) \\ C^{12}(n,n')C^{12*} \\ C^{12}(n,p)B^{12} \end{array}\right\}$$

This greatly complicates the evaluation of the resulting secondary products. According to Bowen et al. (1962, p. 118), the effectiveness of neutron detection in carbon-hydrogen scintillators can be calculated, using the total effective cross section of the neutron-proton interaction and the various partial effective cross sections which contribute to the total effective cross section of the neutron-carbon interaction, if it is assumed that the detection threshold of the electronics used with the scintillator is low enough. For the NE 213 / 52 scintillator used, the thickness of 10 cm, with a molecular number/cm^3 = 0.8804 cm^{-3} and a ratio of 0.548:0.452 H atoms to C atoms give the curves for the neutron detection probabilities in Figure 10. ε_{nH} and ε_{nC} are the proportions of the two atomic species, H and C, in reference to the total chemical response ε_n. In the calculation, the total effective cross sections $\sigma_{H'}$ and $\sigma_{C'}$ were used for the production of a <u>detectable</u> scintillator pulse in the interaction of neutrons with H or C nuclei, respectively. In this

case, this means that $\sigma_{H'}$ and $\sigma_{C'}$ are determined by the electronic threshold which corresponds to a pulse height of 85% of the Compton edge for ^{137}Cs and, accordingly, a pulse height produced by protons with an energy of 1.7 MeV.

It can be seen that at low energies, the chemical response due to hydrogen far exceeds that of carbon. Then ε_{nC} predominates above 30 MeV. At these energies one would get grossly false results if measured pulse height distributions were treated as pure recoil proton spectra in the calculation back to neutron spectra. But since ε_{nC} is the only integral response leading to pulses higher than would correspond to a proton energy of 1.7 MeV, one obtains no information from ε_{nC} about the differential pulse height spectrum, dh/dk. There are as yet only a few measurements for n-C reactions above this pulse height spectrum, but the pulse height spectrum for n-H reactions is relatively well known.

In the following, we shall calculate the differential pulse height spectra generated by the calibration neutron spectra in the apparatus. Only the well-known n-H reactions are considered. By comparing the calculated and the measured spectra, we can then estimate the effect of the n-C reactions.

Let the differential neutron spectrum as a function of the neutron energy, E_n (Figure 5) per deuteron charge, dQ, neutron energy interval dE_n, and solid angle $d\Omega$ be

$$\frac{dN}{dQ\, dE_n\, d\Omega}(E_n) = q(E_n)$$

If $\varepsilon_{geo}(E_n)$ is the geometrical response capability, $\varepsilon_{nH}(E_n)$ is the chemical response, $f(E_p, E_n)$ the probability that a secondary particle has an energy E_p in the range $0 \leq E_p \leq E_n$, $d\Omega$ the solid angle for the experiment and Q the charge of all

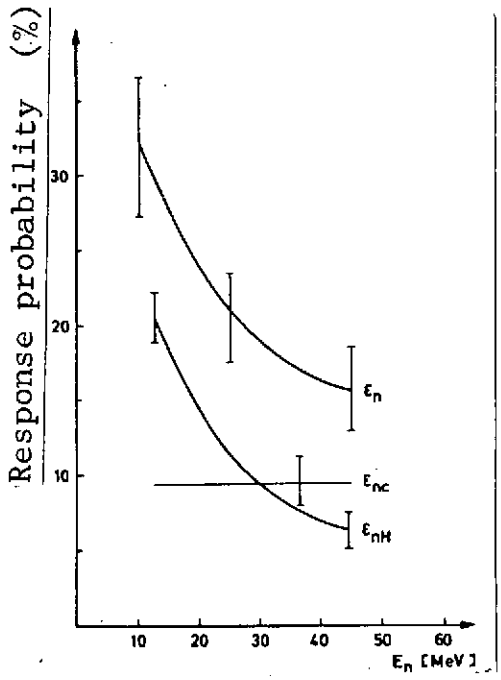

Figure 10. The neutron detection efficiency of a layer of 10 cm NE 213 scintillator, taking into account only H atoms (ε_{nH}), only C atoms (ε_{nC}), and H atoms as well as C atoms (ε_n).

the incident deuterons generating the spectrum, then for the incident neutron spectrum $g(E_n)$ we have

$$\frac{dh(E_p)}{dE_p} = \int_0^\infty \int_\Omega \int_Q f(E_p, E_n)\, \varepsilon_{geom}(E_n)\, \varepsilon_{nH}(E_n)\, g(E_n)\, dE_n\, d\Omega\, dQ$$

for the measured differential pulse height spectrum of the secondary particles, $dh(E_p)/dE_p$, with

$$\int_0^{E_n} f(E_p, E_n)\, dE_p = 1$$

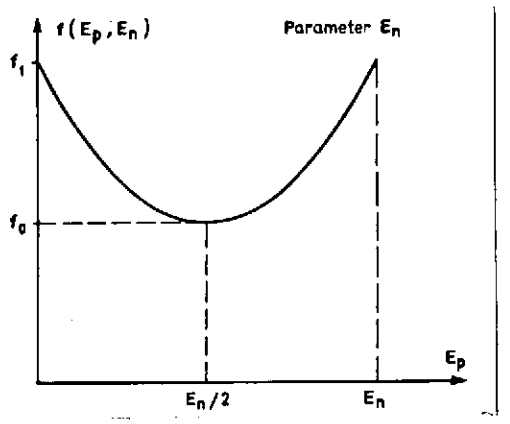

Figure 11. Approximation of the probability, $f(E_p, E_n)$ by a parabola (see text).

The following quantities are important for the numerical calculation:

a) The solid angle of the experiment: $2.46 \cdot 10^{-6}$ sr.

b) The number of incident deuterons, D_1 or D_2, according to the table. As the two measuring methods gave different values for the deuteron intensity, the curves were calculated for both intensities.

c) The response ε_{null} as a function of E_n according to Figure 10. As a good approximation, we can set $\varepsilon_{geoll} = 1$ for the calibration measurement.

d) The probability $f(E_p, E_n)$ can, according to measurements by Barschall and Taschek (1949) and Hadley, Kelly et al. (1949), be approximated by a parabola of the following shape (Figure 11):

$$f(E_p, E_n) = a E_p^2 + b E_p + f_1 \quad \text{with} \quad E_n = -b/a$$

The peak of the parabola can be calculated as

$$f_0 = (4af_1 - b^2)/4a .$$

The ratio, $z = f_1/f_o(E_n)$ was interpolated from the measurements of Hadley, Kelly et al. (1949) and Barschall and Taschek (1949) for all the intermediate energies.

The condition for area normalization under the parabolic segments is

$$\int_0^{E_n} (a E_p^2 + b E_p + f_1)\, dE_p = 1$$

With $a = -b/E_n$ it follows that

$$\frac{b}{6} E_n^2 + f_1 E_n = 1$$

Thus, the parabolas can be calculated from the following equations: / 53

$$f_1 = \frac{3}{E_n(1+2/Z)}$$
$$b = \left(\frac{1}{2} - 1\right)\frac{4 f_1}{E_n}$$
$$a = -\frac{b}{E_n}$$

Figure 12 shows the parabolas for $E_n = (12.5 + 2n)$ MeV with $n = 0, 1, 2, \ldots 17$. In this way, the integral of Equation (1) was calculated numerically in steps.

Figure 13 shows the curves for Be and Au targets, calculated on the basis of n-p processes. The total number of deuterons, D_1, from the ^{22}Na measurement enters into the curves designated with (1), and the number of deuterons, D_2, from the ^{24}Na measurement enters into the curves designated with (2). The slopes of the calculated curves are considerably greater than those of the measured spectra. This indicates that the neglect of the carbon in the scintillator leads to large errors.

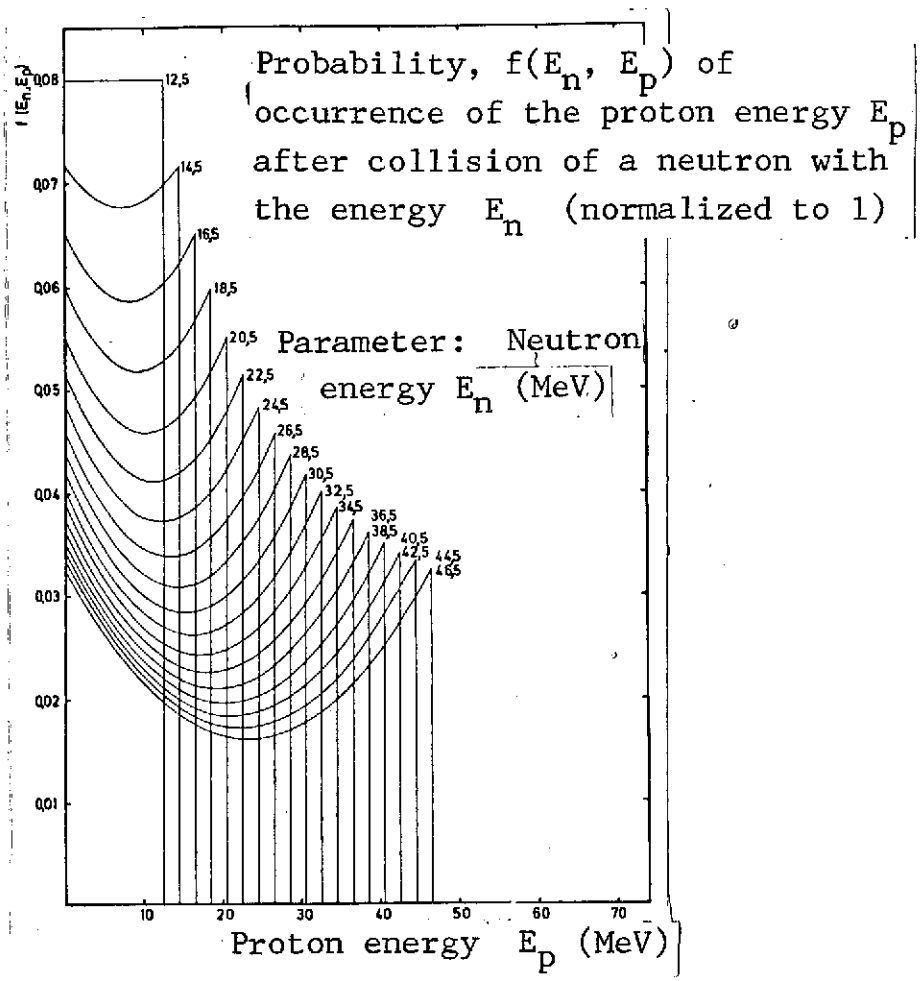

Figure 12. Normalized probability $f(E_n, E_p)$ of the occurrence of the proton energy E_p after the collision of a neutron (neutron energy E_n) with a proton at rest.

From the effective cross sections σ_C and σ_H we can see that for energies $\gtrsim$ 15 MeV, it is practically only neutron reactions with hydrogen which have a part in the heights of the pulses of the secondary spectrum. Therefore, the calculated curves must agree with the measured spectrum, with respect to absolute value and slope, below 12 MeV, if the incident

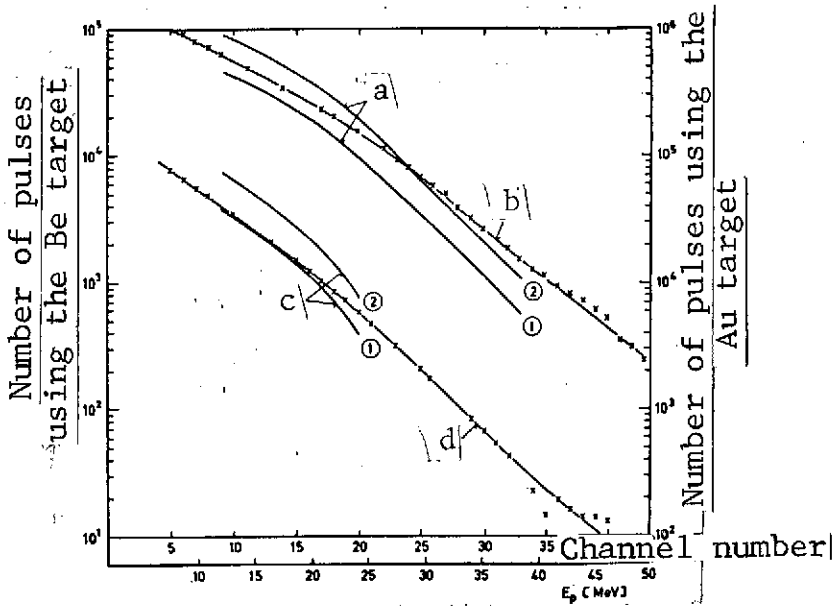

Figure 13. Comparison of the measured differential pulse height spectra of the Be and Au targets with the pulse height spectra calculated assuming only recoil protons.

a - Calculated differential pulse height spectra for Be target
b - Measured differential pulse height spectrum for Be target
c - Calculated differential pulse height spectra for Au target
d - Measured differential pulse height spectrum for Au target

neutron spectrum rises fast enough toward lower energies. Then the high-energy neutrons make hardly any contribution at the low energies because of their small number.

The errors which enter into the theoretical calculation are first determined by measurements. The deuteron intensity is known only within a factor of 2. The errors in the neutron calibration spectrum are 5% in the energy scale and 10% in the absolute intensity at neutron energies about 12 MeV. The relative error becomes larger at higher energies. It is 15% in the Be irradiation for E_n = 40 MeV and 30% in the Au irradiation for E_n = 30 MeV. There is also a certain uncertainty due to the fact that the intensity of the calibration

spectrum for E_d = 46.35 MeV was linearly interpolated between the calibration spectra for E_d = 40.0 and E_d = 53.8 MeV. On the other hand, the assumption of parabolas as probability distributions does not enter strongly into the calculation. Had one used instead rectangles of the same area, the course of the curves at low energies would not have been very different. At 38.5 MeV (Be value) the intensity would have been 20% lower, and only 12% at 26.5 MeV (Au value).

At low energies ($\lesssim$15 MeV) the pulse height spectra (1) and (2), calculated on the basis of the n-p process for both the Au and the Be targets, agree with the measured spectra within the limits of error. On the other hand, at higher energies the measured spectra cannot any longer be explained by recoil protons alone. The secondary spectra were calculated experimentally for constant chemical response, $\varepsilon_n = 0.15$ and the deuteron intensities for Be and Au, D, given above. They give quite good agreement with the measurements at higher energies. This indicates that the carbon contributes decisively to production of the secondary spectrum at these energies. This is plausible, as ε_{nC} exceeds ε_{nH} above 30 MeV. The downward bend in the curves for ε_n = 0.15 can be avoided if one uses the value of $\varepsilon_n = \varepsilon_{nH}$ in the range where ε_{nH} exceeds the value of $\varepsilon_n = 0.15$. That is the case for energies $E_p \lesssim 18.5$ MeV. / 54

Figure 14 contains curves (1) and (2) drawn for such a combined response for the deuteron intensities D_1 and D_2. In this way, one obtains outstanding agreement between the measured and calculated secondary spectra.

The measurements show the importance of the n-C reactions in scintillators at high neutron energies They are opposed to the assumption of Grannan, Koga et al. (1972) in calibrating their spectrometer for neutrons of 2 MeV to 100 MeV, that

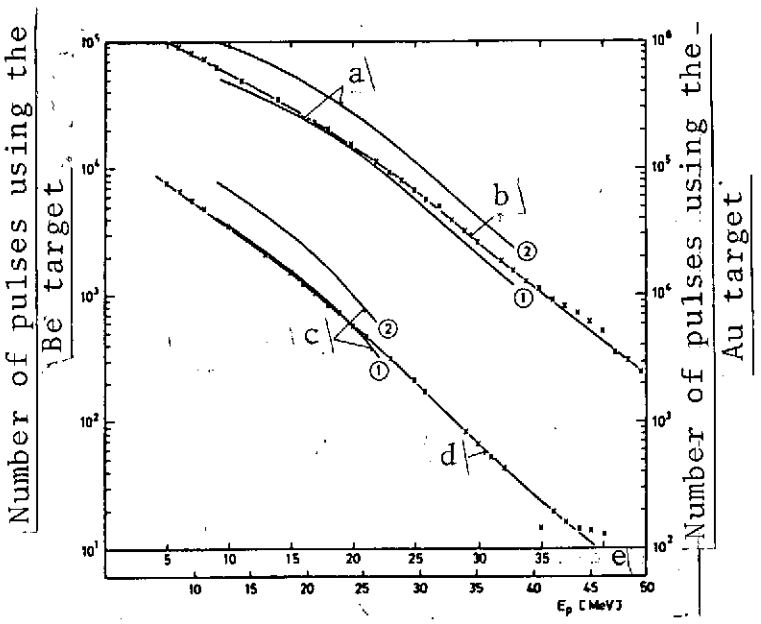

Figure 14. Like Figure 13, but instead of using η_n (Figure 10) for all neutron energies, η_n has been set to 0.15 for $E_p > 18.5$ MeV and to η_H for $E_p \leq 18.5$ MeV.

a - Calculated differential pulse height spectra for the Be target

b - Measured differential pulse height spectrum for the Be target

c - Calculated differential pulse height spectra for Au target

d - Measured differential pulse height spectrum for Au target

e - Channel number

---

the percentage of all detected events which are due to inelastic neutron collisions with carbon is small. Grannan, Koga et al. support their assumption primarily upon the low effectiveness of the conversion of energy into visible light by slowly moving heavy ions.

On the other hand, our measurements agree well with those of Edelstein, Russ et al. (1972), who have found that for neutron energies $E_n \gtrsim 25$ MeV it is principally recoil protons, and for $E_n \gtrsim 50$ MeV, principally inelastic carbon reactions which determine the detection probability.

5. Summary

An apparatus consisting of two scintillation counters for measurement of neutrons up to 50 MeV is described and built. It was irradiated at the cyclotron in Karlsruhe in two series of measurements, using neutrons with known energy spectra in the range $12 \leq E_n \leq 40$ MeV, so that the resulting secondary spectra could be measured. An electronic pulse shape discrimination system was adjusted so that gamma quanta and neutrons could be separated above 20 MeV.

The organic scintillator NE 213, with which the neutron detection was done, consists of 54.8% H atoms and 45.2% C atoms. As the recoil proton spectra resulting from scattering of neutrons by H atoms are largely known, their contribution to the measured secondary spectrum could be eliminated. One obtains the following results for the scintillator NE 213:

1. The secondary spectrum is due solely to recoil protons below E_n = 15 MeV.
2. At E_n = 25 MeV the measured spectrum is higher by a factor of 1.3 than the spectrum calculated by considering only the recoil protons. At 35 MeV the factor is 1.8.
3. If one introduces an effective chemical response of $\varepsilon_n = 0.15$ in the region $18 \leq E_n \leq 40$ MeV and takes the value reported in the literature for hydrogen for the response below 18 MeV, one obtains outstanding agreement between the measured and the calculated secondary spectrum. The constancy of the response in the specified energy range reflects the constancy of the effective cross section, σ_C for neutron reactions with carbon in the scintillator, leading to generation of a detectable scintillator pulse above a proton energy of 1.7 MeV.

We thank Prof. Dr. E. Bagge for stimulating interest in the performance of this work in his Institute. We also thank Engineer G. Fleissner for his untiring help and his careful work in developing the electronics for the apparatus.

We thank Dr. G. Schatz and Dr. G. W. Schweimer of the cyclotron at the Karlsruhe Nuclear Research Center. Their help made the neutron measurements at Karlsruhe possible.

This work was made possible by support from the German Research Society.

REFERENCES

1. Barschall, H. H. and R. F. Taschek. Angular Distribution of 14 MeV Neutrons Scattered by Protons. Phys. Rev. Vol. 75, 1949, pp. 1819-1822.

2. Biermann, L., O. Haxel and A. Schlüter. Neutral Ultra-radiation from the Sun. Z. Naturforschg. Vol. 6a, 1951, pp. 47-48.

3. Bowen, P. H., G. C. Cox, G. B. Huxtable, A. Langsford, J. P. Scanlon, G. H. Stafford and J. J. Thresher. A Method of Measuring the Efficiencies for Detecting High Energy Neutrons Organic Scintillators. Nucl. Instr. Meth. Vol. 17, 1962, pp. 117-122.

4. Busse, I. Construction of a Spectrometer to Measure the Intensity and the Energy Spectrum of Fast Neutrons of Cosmic Radiation, using Pulse Shape Discrimination. Diplomarbeit Kiel, 1967.

5. Claflin, E. S. and R. S. White. Injection of Protons into the Radiation Belt by Solar Neutron Decay. J. Geophys. Res. Vol. 75, 1970, pp. 1257-1262.

6. Chupp, E. L. Gamma Ray and Neutron Emissions from the Sun. Space Sci. Rev., Vol. 12, 1971, pp. 486-525.

7. Edelstein, R. M., J. S. Russ, R. C. Thatcher, M. Elfield, E. L. Miller, N. W. Reay, N. R. Stanton, M. A. Abolins, M. T. Lin, K. W. Edwards and D. R. Gill. Calibration of the Neutron Detection Efficiency of a Plastic Scintillator, 1 to 200 MeV. Necl. Instr. Meth. Vol. 100, 1972, pp. 355-359.

8. Farley, T. A., A. D. Tomassian and M. Walt. Source of High Energy Protons in the Van Allen Radiation Belt. Phys. Rev. Lett. Vol. 25, 1970, pp. 47-49.

9. Göllnitz, H., E. Heidbreder, K. Pinkau, C. Reppin, V. Schönfelder and R. Gorenflo. Design of a Neutron Scattering Chamber Using Monte Carlo Calculations. Nucl. Instr. Meth., Vol. 74, 1969, pp. 109-122.

10. Grannan, R. T., R. Koga, W. A. Millard, A. M. Preszler, G. M. Simnett and R. S. White. A Large Area Detector for Neutrons between 2 and 100 MeV. Univ. of Calif. Preprint IGPP-UCR-72-2, 1972

11. Hadley, J., E. Kelly, C. Leith, E. Segre, L. Wiegand and H. York. Experiments on N-P Scattering with 90- and 40-MeV Neutrons. Phys. Rev. Vol. 75, 1949, pp. 351-363.

12. Hunt, J. B., C. A. Baker, C. J. Batty, P. Ford, E. Friedmann and L. E. Williams. Medium Energy Neutron Time-Of-Flight Spectrometer, II. Neutron Detection Efficiency of Organic Scintillators. Nucl. Instr. Meth. Vol. 85, 1970, pp. 269-276.

13. Kinbara, S. and T. Kumahara. A General Purpose Pulse Shape Discriminating Circuit. Nucl. Instr. Meth. Vol. 70, 1969, pp. 173-182.

14. Onge, R. N. S. and J. A. Lockwood. A Simple High Resolution Pulse Shape Discriminator. Nucl. Instr. Meth. Vol. 69, 1969, pp. 25-28.

15. Preszler, A. M., G. M. Sinnett and R. S. White. Earth Albedo Neutrons from 10 to 100 MeV. Univ. of Calif. Preprint, 1972.

16. Roelof, E. C. Effect of the Interplanetary Magnetic Field on Solar Neutron-Decay Protons. J. Geophys. Res. Vol. 71, 1966, pp. 1305-1317.

17. Schweimer, G. W. Study of Deuteron Breakup Neutrons with a Time-Of-Flight Method at 50 MeV. Report No. 504 of the Karlsruhe Nuclear Research Center, 1966.

18. White, R. S., S. H. Moon, A. M. Preszler and G. M. Simnett. Earth Albedo and Solar Neutrons. No. 15. COSPAR Meeting, Madrid, 1972.

Translated for National Aeronautics and Space Administration under contract No. NASw 2483, by SCITRAN, P. O. Box 5456, Santa Barbara, California, 93108.